ASME Journal of Applied Mechanics
Online journal at:
https://asmedigitalcollection.asme.org/appliedmechanics

On the Nature of Symmetrical Contacts of a Beam Impacting a Rigid Wall

V. Denoël[1]
Structural & Stochastic Dynamics,
University of Liège,
4000 Lige, Belgium;
Department of Civil and Environmental
Engineering,
Stanford University,
Stanford, CA 94305
e-mail: v.denoel@uliege.be

E. Detournay
Department of Civil, Environmental
and Geo-Engineering,
University of Minnesota,
Minneapolis, MN 55455
e-mail: detou001@umn.edu

The impact of a compliant structure against a rigid obstacle is governed by multiple time and spatial scales, ranging from rapid local deformations and stress wave propagation to slower global motions. This interaction presents significant challenges for numerical methods, particularly in resolving the immediate postimpact response and contact dynamics. In this study, we focus on the impact of a beam on a rigid obstacle as a minimal yet representative example of such multiscale phenomena. A local asymptotic solution is derived for the short-time response. At leading order, the analysis reveals two distinct contact patterns governed by the ratio of the impact velocity to the beam curvature at the contact point: a single concentrated force whose intensity decays with the inverse square root of time or a pair of traveling forces that move away from each other at a rate inversely proportional to the square root of time. Notably, in the latter case, the beam segment between the traveling forces remains stationary, posing challenges for numerical methods based on penetration conditions. These findings highlight the utility of asymptotic methods in capturing the singular and bifurcated nature of contact forces in multiscale impact problems. The solution can be used to improve or provide a benchmark for assessing numerical approaches in the impact analysis of compliant beam structures with rigid walls. [DOI: 10.1115/1.4070020]

Keywords: discrete contact, continuous contact, self-similar solution, Volterra equation of the first kind, free boundary problem, dynamics, impact, wave propagation

1 Introduction

The impact of a compliant structure against a rigid obstacle is a complex phenomenon characterized by multiple time and spatial scales [1]. On short time scales, rapid local deformations and stress wave propagation dominate, while on longer time scales, slower global motions become more prominent. Similarly, spatial scales range from short localized contact regions, where stress gradients are steep, to the larger structural dimensions influenced by boundary conditions and governing multimodal responses. These scales interact in ways that present challenges for numerical modeling, particularly in accurately capturing the immediate response after impact and resolving the details near the contact point.

The study of contact dynamics in flexible beam systems has evolved significantly, starting with foundational analytical models and progressing to advanced numerical and experimental approaches. Early works [2,3] provided pioneering analytical solutions for beam impacts, focusing on infinite and elastic beams under various loading and contact conditions. These studies established critical insights into energy transfer and stress distribution during localized impact events. Theoretical solutions of the pointwise impact on Bernoulli, Rayleigh, or Timoshenko beam are now available in textbooks [4]. Zhou and Schonberg [5] critiqued global-local methods for impact analysis, among which the use of assumptions of Hertzian contact, and developed analytical solutions for a spherical impactor on a flexible beam as a solution of a Volterra equation.

The introduction of numerical methods marked a significant advancement. Initial simulations utilized finite element methods to discretize beams and model interactions with rigid walls, relying on penalty methods or simplified contact formulations. Bauchau [6] was instrumental in improving these techniques, addressing the challenges of transient interactions and introducing robust computational frameworks for dynamic contact scenarios. Nonsmooth time integration schemes tailored for flexible multibody systems under unilateral constraints were also advanced [7]. Simultaneously, the study of friction and more complex contact scenarios gained prominence. Durville [8] modeled contact-friction behavior in elastic beam assemblies, and Bertails-Descoubes et al. [9] introduced nonsmooth Newton solvers to capture Coulomb friction with high accuracy. These works bridged computational mechanics with physical phenomena, enhancing model reliability. Unlike in previous dissipative schemes [10], incorporating energy preservation and stability into numerical schemes became a focal point with works like Lens and Cardona [11], who developed nonlinear beam elements within energy-preserving frameworks.

Advanced numerical approaches highlight the significant challenges posed by multiple scales in efficiently computing the response immediately after impact, particularly near the point of contact. In contrast, the separation of time and spatial scales in

[1]Corresponding author.

Manuscript received July 5, 2025; final manuscript received September 1, 2025; published online xx xx, xxxx. Tech. Editor: Pradeep Sharma.

the moments following impact can often be handled more effectively through analytical derivations. A prime example of such multiscale behavior is the impact of a beam on a rigid obstacle. This article explores this scenario by deriving a local asymptotic solution valid for small times after impact. At these short timescales, the separation of scales ensures that the solution near the contact point depends solely on the impact velocity and the beam's curvature at the moment and location of impact.

Despite its simplicity, this problem reveals two distinct response patterns, determined by the impact velocity and the beam curvature. These parameters act as bifurcation parameters that govern the nature of the contact force. The contact force may manifest as either a fixed, discrete force or a pair of traveling forces. The discrete force decreases over time following an inverse square root law, while the distance between the two traveling forces grows with the square root of time. These contact patterns are a reminiscence of the nonsmooth static response of beams pressed on walls as was observed in various problems including modeling paper insertion in a toner [12], endoscopic insertion of a flexible beam in a conduit [13], determining the drillstring configuration in a borehole [14] or constrained buckling [15,16].

The article begins in Sec. 2 with the formulation of the beam impact problem, introducing the governing equations, complementarity condition, and initial and boundary conditions. Section 3 examines the slow and fast timescales of the problem, establishing an early matching between their asymptotic solutions and interpreting the small parameter ε. Section 4 derives the leading-order impulse response function and basic solutions for two contact patterns: single-point contact and double symmetric contact. Section 5 develops perturbation solutions, satisfying complementarity conditions for both scenarios. Section 6 discusses the implications, illustrating contact behaviors and potential extensions beyond leading-order analysis.

2 Problem Formulation

The impact of a symmetrical beam with uniform bending stiffness EI, uniform mass per unit length μ, and total length $2L$, subjected to a symmetrically distributed external forcing per unit length $p(x, t)$, is governed by

$$\mu\partial_t^2 y(x,t) + \mathrm{EI}\partial_x^4 y(x,t) = p(x,t) - r(x,t) \tag{1}$$

where $y(x, t)$ is the transverse position at abscissa x and time t, measured from a fixed reference frame, see Fig. 1(*a*). This equation is to be supplied with appropriate initial and boundary conditions and is subject to the complementarity condition:

$$0 \le r(x,t) \perp y(x,t) \le 0 \tag{2}$$

This condition translates that the unilateral contact is such that the beam does not penetrate the straight and infinitely rigid barrier located on the axis $y = 0$ and that an a priori unknown (possibly distributed) positive reaction pressure $r(x, t)$ develops in order to avoid this penetration. Due to the linearity of the governing equation and to the symmetry of the beam geometry and external forcing, the beam deforms symmetrically. Starting from initial conditions at time $t_0 < 0$, this well-posed large-scale problem is easily solved with traditional tools of smooth dynamics [17] on $(x, t) \in [-L; L] \times [t_0; 0]$ until a contact is initiated. The origin of time and that of the space frame are chosen in such a way that this first contact takes place at time $t = 0$ and abscissa $x = 0$. As will be seen next, the boundary conditions are not relevant as long as the short time solution is sought. For instance, a simply supported beam could be considered, i.e., $y(\pm L, t) = -c$ and $\partial_x^2 y(\pm L, t) = 0$, where c is a clearance. In this study, we develop an analytical solution of this problem by matching asymptotic solutions in the far-field, and in the neighborhood of the contact at short time after the contact is initiated. Before contact occurs, the governing equation is obtained by discarding the reaction $r(x, t)$ on the wall

$$\mu\partial_t^2 y_0 + \mathrm{EI}\partial_x^4 y_0 = p \tag{3}$$

and is solved with standard tools of linear structural dynamics. Then, as soon as a contact is initiated, at time $t = 0$ and abscissa $x = 0$, the complete governing equation (1) needs to be considered together with the complementarity equation. This contact develops over a domain $\mathcal{D}$, which might be a single point $\{0\}$, two symmetrical points $\{-\lambda_c, +\lambda_c\}$, or a finite domain $[-\lambda_c, +\lambda_c]$. Accordingly, it involves either one- or two-point reactions on the wall, with possible development of a distributed contact pressure. This is similar to previous observations in a static configuration [12,13]. In the first case, the contact reaction takes the form of a Dirac, $r(x, t) = R(t)\delta(x)$, and the reaction force $R(t)$ evolves in time in such a way to satisfy the complementarity condition, i.e., $y(0, t) = 0$, at least until the contact is lost. In the second and third cases, two-point reactions move away from each other and possibly reveal a distributed pressure in-between; by doing so, they leave a portion of beam at rest along the domain $\mathcal{D}$, see Fig. 1(*b*). This is a typical feature of a free boundary problem.

3 Slow and Fast Dynamics

It is assumed that the two terms in the right-hand side of the governing equation (1) evolve on different timescales, otherwise a numerical approach would be more efficient than the following matching asymptotic derivation. We therefore anticipate the solution of the problem by introducing two timescales. They are related to the slow oscillations of the beam due to slow $p(x, t)$ and the fast wave propagation posterior to the impact associated with fast $r(x, t)$.

3.1 Slow Dynamics. The homogenous form of the governing equation (1) reveals the main parameter of this problem, $\sqrt{\mathrm{EI}/\mu}$, which has dimensions of a diffusion coefficient ($\mathrm{L}^2\mathrm{T}^{-1}$). Together with the span L of the beam, considered as the macroscopic

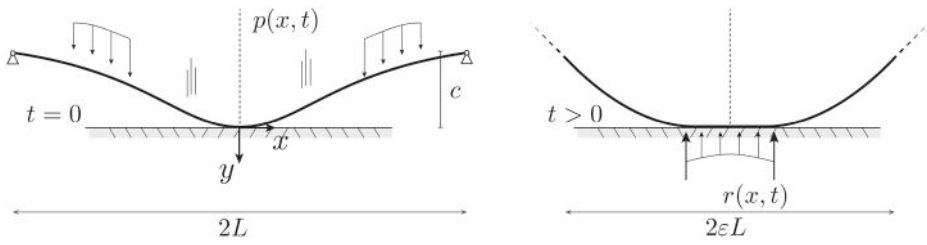

Fig. 1 Schematic of the considered problem. Left: At a large scale, a vibrating beam with its own boundary conditions symmetrically impacting a rigid wall. Right: Close-up view in the vicinity of the contact, where a possibly distributed reaction pattern takes place at short time post impact.

On the Nature of Symmetrical Contacts of a Beam Impacting a Rigid Wall

V. Denoël [a,b], *E. Detournay* [c]

[a] University of Liège, Structural & Stochastic Dynamics, Belgium

[b] Stanford University, Department of Civil and Environmental Engineering, USA

[c] University of Minnesota, Department of Civil, Environmental and Geo-Engineering, Minneapolis, USA

Abstract

The impact of a compliant structure against a rigid obstacle is governed by multiple time and spatial scales, ranging from rapid local deformations and stress wave propagation to slower global motions. This interaction presents significant challenges for numerical methods, particularly in resolving the immediate post-impact response and contact dynamics. In this study, we focus on the impact of a beam on a rigid obstacle as a minimal yet representative example of such multi-scale phenomena. A local asymptotic solution is derived for the short-time response. At leading order, the analysis reveals two distinct contact patterns governed by the ratio of the impact velocity to the beam curvature at the contact point: a single concentrated force whose intensity decays with the inverse square root of time or a pair of traveling forces that move away from each other at a rate inversely proportional to the square root of time. Notably, in the latter case, the beam segment between the traveling forces remains stationary, posing challenges for numerical methods based on penetration conditions. These findings highlight the utility of asymptotic methods in capturing the singular and bifurcated nature of contact forces in multi-scale impact problems. The solution can be used to improve or provides a benchmark for assessing numerical approaches in the impact analysis of compliant beams structures with rigid walls.

Keywords: discrete contact ; continuous contact ; self-similar solution; Volterra equation of the first kind ; free boundary problem

1 Introduction

The impact of a compliant structure against a rigid obstacle is a complex phenomenon characterized by multiple time and spatial scales [1]. On short time scales, rapid local deformations and stress wave propagation dominate, while on longer time scales, slower global motions become more prominent. Similarly, spatial scales range from short localized contact regions, where stress gradients are steep, to the larger structural dimensions influenced by boundary conditions and governing multimodal responses. These scales interact in ways that present challenges for numerical modeling, particularly in accurately capturing the immediate response after impact and resolving the details near the contact point.

The study of contact dynamics in flexible beam systems has evolved significantly, starting with foundational analytical models and progressing to advanced numerical and experimental approaches. Early works [2, 3] provided pioneering analytical solutions for beam impacts, focusing on infinite and elastic beams

under various loading and contact conditions. These studies established critical insights into energy transfer and stress distribution during localized impact events. Theoretical solutions of the pointwise impact on Bernoulli, Rayleigh or Timoshenko beams are now available in textbooks [4]. Zhou and Schonberg [5] critiqued global-local methods for impact analysis, among which the use of assumptions of Hertzian contact, and developed analytical solutions for a spherical impactor on a flexible beam as a solution of a Volterra equation.

The introduction of numerical methods marked a significant advancement. Initial simulations utilized finite element methods to discretize beams and model interactions with rigid walls, relying on penalty methods or simplified contact formulations. Bauchau [6] was instrumental in improving these techniques, addressing the challenges of transient interactions and introducing robust computational frameworks for dynamic contact scenarios. Nonsmooth time integration schemes tailored for flexible multibody systems under unilateral constraints were also advanced [7]. Simultaneously, the study of friction and more complex contact scenarios gained prominence. Durville [8] modeled contact-friction behavior in elastic beam assemblies, and Bertails-Descoubes et al. [9] introduced nonsmooth Newton solvers to capture Coulomb friction with high accuracy. These works bridged computational mechanics with physical phenomena, enhancing model reliability. Unlike in previous dissipative schemes [10], incorporating energy preservation and stability into numerical schemes became a focal point with works like Lens and Cardona [11], who developed nonlinear beam elements within energy-preserving frameworks.

Advanced numerical approaches highlight the significant challenges posed by multiple scales in efficiently computing the response immediately after impact, particularly near the point of contact. In contrast, the separation of time and spatial scales in the moments following impact can often be handled more effectively through analytical derivations. A prime example of such multi-scale behavior is the impact of a beam on a rigid obstacle. This paper explores this scenario by deriving a local asymptotic solution valid for small times after impact. At these short timescales, the separation of scales ensures that the solution near the contact point depends solely on the impact velocity and the beam's curvature at the moment and location of impact.

Despite its simplicity, this problem reveals two distinct response patterns, determined by the impact velocity and the beam curvature. These parameters act as bifurcation parameters that govern the nature of the contact force. The contact force may manifest as either a fixed, discrete force or a pair of traveling forces. The discrete force decreases over time following an inverse square root law, while the distance between the two traveling forces grows with the square root of time. These contact patterns are a reminiscence of the nonsmooth static response of beams pressed on walls as was observed in various problems including modeling paper insertion in a toner [12], endoscopic insertion of a flexible beam in a conduit [13], determining the drillstring configuration in a borehole [14] or constrained buckling [15, 16].

The paper begins in Section 2 with the formulation of the beam impact problem, introducing the governing equations, complementarity condition, and initial and boundary conditions. Section 3 examines the slow and fast timescales of the problem, establishing an early matching between their asymptotic solutions and interpreting the small parameter ε. Section 4 derives the leading-order impulse response function and basic solutions for two contact patterns: single-point contact and double symmetric contact. Section 5 develops perturbation solutions, satisfying complementarity conditions for both scenarios. Section 6 discusses the implications, illustrating contact behaviors and potential extensions beyond leading-order analysis.

2 Problem formulation

The impact of a symmetrical beam with uniform bending stiffness EI, uniform mass per unit length μ and total length $2L$, subjected to a symmetrically distributed external forcing per unit length $p(x,t)$ is governed by

$$\mu\partial_t^2 y(x,t) + EI\partial_x^4 y(x,t) = p\,(x,t) - r(x,t) \tag{1}$$

where $y(x,t)$ is the transverse position at abscissa x and time t, measured from a fixed reference frame, see Figure 1-a. This equation is to be supplied with appropriate initial and boundary conditions and is subject to the complementarity condition

$$0 \leq r(x,t) \perp y(x,t) \leq 0. \tag{2}$$

This condition translates that the unilateral contact is such that the beam does not penetrate the straight and infinitely rigid barrier located on the axis $y = 0$ and that an *a priori* unknown (possibly distributed) positive reaction pressure $r(x,t)$ develops in order to avoid this penetration. Due to the linearity of the governing equation and to the symmetry of the beam geometry and external forcing, the beam deforms symmetrically. Starting from initial conditions at time $t_0 < 0$, this well-posed large scale problem is easily solved with traditional tools of smooth dynamics [17] on $(x,t) \in [-L;L] \times [t_0;0]$ until a contact is initiated. The origin of time and of the space frame are chosen in such a way that this first contact takes place at time $t = 0$ and abscissa $x = 0$. As seen next, the boundary conditions are not relevant as long as the short time solution is sought. For instance, a simply supported beam could be considered, i.e. $y(\pm L,t) = -c$ and $\partial_x^2 y(\pm L,t) = 0$, with c a clearance.

In this study, we develop an analytical solution of this problem by matching asymptotic solutions in the far-field, and in the neighborhood of the contact at short time after the contact is initiated. Before contact occurs, the governing equation is obtained by discarding the reaction $r(x,t)$ on the wall

$$\mu\partial_t^2 y_0 + EI\partial_x^4 y_0 = p \tag{3}$$

and is solved with standard tools of linear structural dynamics. Then, as soon as a contact is initiated, at time $t = 0$ and abscissa $x = 0$, the complete governing equation (1) needs to be considered together with the complementarity equation. This contact develops over a domain $\mathcal{D}$ which might be a single point $\{0\}$, two symmetrical points $\{-\lambda_c, +\lambda_c\}$ or a finite domain $[-\lambda_c, +\lambda_c]$. Accordingly it involves either one or two point reactions on the wall, with possible development of a distributed contact pressure. This is similar to previous observations in a static configuration [12, 13]. In the first case, the contact reaction takes the form of a Dirac, $r(x,t) = R(t)\delta(x)$, and the reaction force $R(t)$ evolves in time in such a way to satisfy the complementarity condition, *i.e.* $y(0,t) = 0$, at least until the contact is lost. In the second and third cases, two point reactions move away from each other and possibly reveal a distributed pressure in-between; by doing so they leave a portion of beam at rest along the domain $\mathcal{D}$, see Figure 1-b. This is a typical feature of a free boundary problem.

3 Slow and fast dynamics

It is assumed that the two terms in the righthand side of the governing equation (1) evolve on different timescales, otherwise a numerical approach would be more efficient than the following matching asymptotic derivation. We therefore anticipate the solution of the problem by introducing two timescales respectively. They are related to the slow oscillations of the beam due to slow $p(x,t)$ and the fast wave propagation posterior to the impact associated with fast $r(x,t)$.

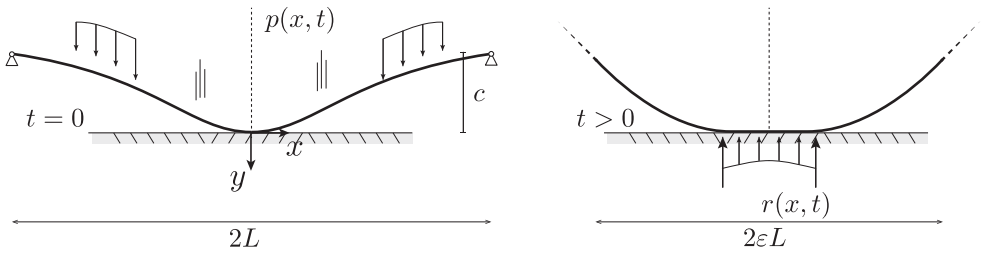

Fig. 1: Schematic of the considered problem. Left: at large scale, a vibrating beam with its own boundary conditions symmetrically impacting a rigid wall. Right: close-up view in the vicinity of the contact, where a possibly distributed reaction pattern takes place at short time post impact.

3.1 Slow dynamics

The homogenous form of the governing equation (1) reveals the main parameter of this problem, $\sqrt{EI/\mu}$, which has dimensions of a diffusion coefficient ($\mathsf{L}^2\mathsf{T}^{-1}$). Together with the span L of the beam, considered as the macroscopic characteristic length $L^\star$, it defines a slow timescale

$$T^\star = \sqrt{\frac{\mu L^{\star 4}}{EI}} \tag{4}$$

which is also related to the fundamental period of beam oscillations. The transverse displacement of the beam is scaled by a characteristic transverse displacement defined by $y^\star = p^\star L^{\star 4}/EI$ where $p^\star$ is a characteristic load per unit length, representative of $p\,(x,t)$. The solution of (3) is the slow response before contact takes place. It is written in the dimensionless form

$$y_0(x,t) = y^\star \Upsilon\left(\frac{x}{L^\star}, \frac{t}{T^\star}\right) \tag{5}$$

where $\Upsilon\,(\cdot,\cdot)$ is a function of order 1.

3.2 Fast dynamics

After the impact (for $t \geq 0$), the governing equation (1) must be solved alongside the complementarity condition (2). Due to the piecewise linear nature of the problem, the solution is expressed as the sum of a slow response, $y_0(x,t)$, and a fast response, $z(x,t)$. Substituting $y(x,t) = y_0(x,t) - z(x,t)$ into (1) and subtracting (3), it is found that the fast response $z(x,t)$ satisfies

$$\mu \partial_t^2 z + EI \partial_x^4 z = r. \tag{6}$$

The fast dynamics take place on a timescale $t^\star$ assumed to be short compared to the macroscopic timescale, i.e. $t^\star = \varepsilon T^\star$ where $\varepsilon \ll 1$ is a small parameter. The corresponding lengthscale is naturally chosen as $\ell^\star = \sqrt{\varepsilon} L^\star$ because of the differentiation orders with respect to time and space in the governing equation, respectively. Introducing the dimensionless time τ and coordinate ξ

$$\tau = t/t^\star \qquad \text{and} \qquad \xi = x/\ell^\star, \tag{7}$$

the governing equation (6) becomes

$$\left(\frac{T^\star}{t^\star}\right)^2 \partial_\tau^2 \frac{z}{y^\star} + \left(\frac{L^\star}{\ell^\star}\right)^4 \partial_\xi^4 \frac{z}{y^\star} = \frac{r}{p^\star} \tag{8}$$

or

$$\partial_\tau^2 \eta + \partial_\xi^4 \eta = \tilde{r} \tag{9}$$

where

$$\eta\left(\xi,\tau\right) = \frac{z\left(\xi\ell^\star,\tau t^\star\right)}{\varepsilon y^\star} \qquad \text{and} \qquad \tilde{r}\left(\xi,\tau\right) = \frac{r\left(\xi\ell^\star,\tau t^\star\right)}{\varepsilon^{-1}p^\star} \tag{10}$$

are the dimensionless displacement and reacting pressure on the wall. In (10), the choice to scale the transverse displacement by $\varepsilon y^\star$ is justified by the distinguished limit obtained later. This indicates that the fast dynamics solution involves small displacements, of order $\varepsilon y^\star$, together with large reacting pressures, of order $\varepsilon^{-1}p^\star$.

3.3 Early matching of solutions

In classical perturbation methods, asymptotic solutions are typically developed separately for the far and near fields and then matched in a subsequent step. However, for the present problem, deriving the near-field solution at the fast time scale is difficult. To simplify the process and avoid deriving the general solution explicitly, we directly anticipate the matching of the fast and slow solutions.

To achieve this, the slow dynamics solution (5) is reformulated using stretched coordinates as

$$\begin{aligned} y_0 &= y^\star \Upsilon\left(\xi\sqrt{\varepsilon},\tau\varepsilon\right) \\ &= y^\star\left[\Upsilon\left(0,0\right) + \sqrt{\varepsilon}\xi\Upsilon'\left(0,0\right) + \varepsilon\left(\frac{\xi^2}{2}\Upsilon''\left(0,0\right) + \tau\dot{\Upsilon}\left(0,0\right)\right)\right. \\ &\quad + \varepsilon\sqrt{\varepsilon}\left(\frac{\xi^3}{6}\Upsilon'''\left(0,0\right) + \xi\tau\dot{\Upsilon}'\left(0,0\right)\right) \\ &\quad \left. + \varepsilon^2\left(\frac{\xi^4}{24}\Upsilon''''\left(0,0\right) + \frac{\xi^2\tau}{2}\dot{\Upsilon}''\left(0,0\right) + \frac{\tau^2}{2}\ddot{\Upsilon}\left(0,0\right)\right) + \mathcal{O}\left(\varepsilon^{5/2}\right)\right] \end{aligned} \tag{11}$$

where the prime $'$ symbol denotes differentiation with respect to the first argument and the dot symbol $\dot{}$ denotes differentiation with respect to the second argument. In this expression, $\Upsilon\left(0,0\right) = \Upsilon'\left(0,0\right) = 0$ and $\Upsilon''\left(0,0\right) \leq 0$ and $\dot{\Upsilon}\left(0,0\right) > 0$ because of the occurrence of the contact at $t = 0$ precisely. If one of these conditions was not met, the contact would not take place at time $t = 0$, or would have taken place before. We also assume that the contact is symmetrical, discarding therefore odd powers in ξ. This also means that *rolling contacts* are not studied in this paper.

Equation (11) therefore simplifies into

$$\frac{y_0}{\varepsilon y^\star} = \frac{\xi^2}{2}\Upsilon''\left(0,0\right) + \tau\dot{\Upsilon}\left(0,0\right) + \varepsilon\left(\frac{\xi^4}{24}\Upsilon''''\left(0,0\right) + \frac{\xi^2\tau}{2}\dot{\Upsilon}''\left(0,0\right) + \frac{\tau^2}{2}\ddot{\Upsilon}\left(0,0\right)\right) + \mathcal{O}\left(\varepsilon^2\right). \tag{12}$$

At leading order (in ε, this is actually why we have chosen $\varepsilon y^\star$ to scale z), the stretched macroscopic solution is therefore governed by the dimensionless curvature of the beam at contact

$$\kappa := -\Upsilon''\left(0,0\right) = -\frac{\partial_x^2 y_0\left(0,0\right) L^{\star 2}}{y^\star}, \tag{13}$$

(notice a minus sign is introduced in this definition so that $\kappa \geq 0$), and the dimensionless impact velocity

$$\nu := \dot{\Upsilon}\,(0,0) = \frac{\partial_t y_0\,(0,0)\,T^\star}{y^\star}. \tag{14}$$

The second order solution involves a higher curvature $\partial_x^4 y_0$, the rate of change of the curvature $\partial_x^2 \partial_t y_0$ and the acceleration $\partial_t^2 y_0$ at impact point. In a dimensionless form, they read

$$\psi := \Upsilon''''\,(0,0) = \frac{\partial_x^4 y_0\,(0,0)\,L^{\star 4}}{y^\star} \quad , \quad \alpha := \ddot{\Upsilon}\,(0,0) = \frac{\partial_t^2 y_0\,(0,0)\,T^{\star 2}}{y^\star}, \tag{15}$$

$$\chi := \dot{\Upsilon}''\,(0,0) = \frac{\partial_x^2 \partial_t y_0\,(0,0)\,L^{\star 2} T^\star}{y^\star}. \tag{16}$$

The velocity ν is strictly positive, $\nu > 0$, while the acceleration α can be either positive (the beam accelerates toward the wall) or negative.

In the following, we will focus on the leading order solution of the problem. This early matching of the inner and outer solutions shows that quantities such as the beam acceleration at the time and location of impact concern higher order corrections to the leading order solution.

3.4 Matching and complementarity conditions

Equation (9) governing the fast dynamics solution taking place near the contact point cannot be supplemented with the boundary conditions of the macroscopic problem. Instead, matching conditions need to be invoked. They need to translate that the total solution $y(x,t) = y_0(x,t) - z(x,t) = y_0(x,t) - \varepsilon\, y^\star \eta(x/\ell^\star, t/t^\star)$ matches the slow dynamics solution $y_0(x,t)$ in the far-field, i.e.

$$\lim_{\xi \to \pm\infty} \eta\,(\xi,\tau) = 0 \qquad ; \qquad \lim_{\xi \to \pm\infty} \partial_\xi \eta\,(\xi,\tau) = 0. \tag{17}$$

Furthermore, on the contact domain $\mathcal{D}$, the complementarity equation requires that $y_0(x,t) - z(x,t) = 0$, that is $\Upsilon\,(\sqrt{\varepsilon}\xi, \varepsilon\tau) - \varepsilon\eta(\xi,\tau) = 0$. Introducing the expansion (12), this condition also reads, in a strict sense,

$$\eta(\xi,\tau) = \nu\tau - \kappa\frac{\xi^2}{2} + \varepsilon\left(\psi\frac{\xi^4}{24} + \chi\frac{\xi^2\tau}{2} + \alpha\frac{\tau^2}{2}\right) + \mathcal{O}(\varepsilon^2) \tag{18}$$

which is readily interpreted as a set of complementarity conditions, each one corresponding to a different scale of the problem.

From a different perspective, a discrete contact transforms into a double or continuous contact as soon as the curvature at contact reaches that of the wall [13, 18]. This condition is formally written by equating the total curvature $\partial_x^2 y(x,t) = \partial_x^2 y_0(x,t) - \partial_x^2 z(x,t)$ to zero, i.e., with dimensionless quantities

$$\Upsilon''\left(\xi\sqrt{\varepsilon}, \tau\varepsilon\right) - \partial_\xi^2 \eta(\xi,\tau) = 0, \tag{19}$$

since the wall is considered to be straight. Substituting for $\Upsilon''\,(\xi\sqrt{\varepsilon}, \tau\varepsilon)$ the same development as in (12), we have

$$\partial_\xi^2 \eta(\xi,\tau) = -\kappa + \varepsilon\left(\frac{\xi^2}{2}\psi + \chi\tau\right) + \mathcal{O}(\varepsilon^2) \tag{20}$$

which expresses, in a weaker sense, the complementarity condition. Both (18) and (20) are used in the sequel, whenever convenient or appropriate.

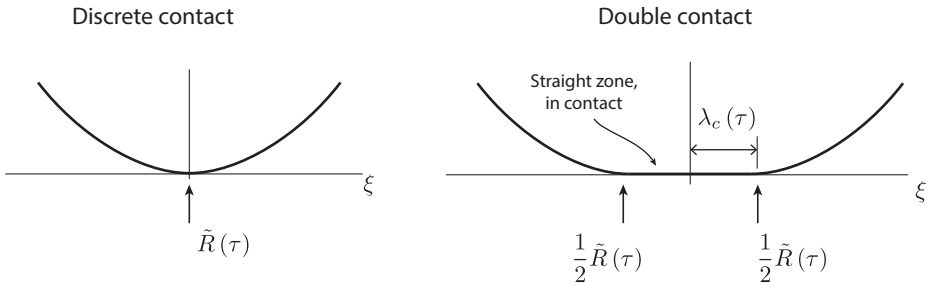

Fig. 2: Two types of contact pattern existing at leading order: discrete contact (point-like contact) and double contact (two discrete forces with a straight zone in contact in-between).

3.5 Interpretation of the small parameter ε

The above considerations show that the problem is formulated at leading order with four parameters, namely EI and μ, together with the curvature $\kappa y^\star/L^{\star 2}$ and velocity $v_o := \nu y^\star/T^\star$ at impact. They are expressed in terms of three independent units (M, L, T), defining a short timescale associated with the fast dynamics problem

$$t^\star = \frac{1}{v_o^2}\sqrt{\frac{EI}{\mu}}. \tag{21}$$

The small parameter introduced before is therefore re-evaluated as

$$\varepsilon = \frac{t^\star}{T^\star} = \left(\frac{L^\star}{v_o T^\star}\right)^2 = \left(\sqrt{\frac{EI}{\mu}}\frac{1}{v_o L^\star}\right)^2. \tag{22}$$

The validity of the solutions developed in this paper, under consideration of separate timescales, requires this parameter to be small ($\varepsilon \ll 1$), which means, a high-velocity impact (v_o) or a long ($L^\star$), heavy (μ) or very flexible beam (EI), relatively speaking.

4 Fundamental solutions of the problem

At leading order, the problem consists therefore in the analysis of an infinitely long beam with constant velocity and curvature impacting a rigid wall. In this scenario, several contact patterns may develop after impact: at leading order, either a discrete contact, either two symmetrical discrete forces moving away from each other, see Figure 2. The detailed expressions of the reactions and position of reaction forces are developed in Sections 5.2 and 5.3. They are based on the fundamental general solutions established in this Section, which are obtained from the impulse response function.

4.1 Impulse response function

The impulse response (or kernel) function $\mathcal{K}(\xi,\tau)$ associated with the vibrations of an infinite beam satisfies the unit impulsive force problem,

$$\partial_\tau^2\mathcal{K} + \partial_\xi^4\mathcal{K} = \delta(\tau)\,\delta(\xi) \tag{23}$$

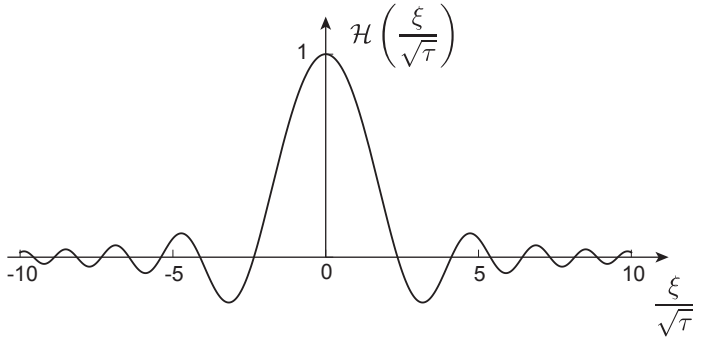

Fig. 3: Self-similar response of an infinite beam under impulsive loading.

for $\xi \in [-\infty; +\infty]$ and with initial rest conditions. The self-similar solution of this well-known problem [2, 4] is

$$\mathcal{K}(\xi, \tau) = \sqrt{\frac{\tau}{2\pi}} \mathcal{H}\left(\frac{\xi}{\sqrt{\tau}}\right) \tag{24}$$

with

$$\mathcal{H}(\beta) = \sqrt{\frac{\pi}{2}} \beta \left[\mathcal{S}\left(\frac{\beta}{\sqrt{2\pi}}\right) - \mathcal{C}\left(\frac{\beta}{\sqrt{2\pi}}\right)\right] + \sqrt{2} \sin\left(\frac{\pi + \beta^2}{4}\right) \tag{25}$$

and where $\mathcal{S}(\cdot)$ and $\mathcal{C}(\cdot)$ stand for Fresnel integrals of the first kind [19]. This function is represented in Fig. 3. The second derivative of $\mathcal{H}(\beta)$, required later, reads

$$\mathcal{H}''(\beta) = \frac{1}{2} \sin\left(\frac{\beta^2}{4}\right) - \frac{1}{2} \cos\left(\frac{\beta^2}{4}\right). \tag{26}$$

4.2 Pattern 1: Discrete contact at $\xi = 0$

In the case of a discrete contact between the beam and the rigid wall, see Fig. 2, the reaction is written as a Dirac function, $\tilde{r}(\xi, \tau) = \tilde{R}(\tau)\, \delta(\xi)$, and the generic governing equation reads

$$\partial_\tau^2 \eta + \partial_\xi^4 \eta = \tilde{R}(\tau)\, \delta(\xi) \tag{27}$$

where $\tilde{R}(\tau)$ will be determined from the complementarity condition. The solution of this equation is written as a convolution of the point reaction and the impulse response function

$$\eta(\xi, \tau) = \int_0^\tau \tilde{R}(\bar{\tau})\, \mathcal{K}(\xi, \tau - \bar{\tau})\, d\bar{\tau} = \frac{1}{\sqrt{2\pi}} \int_0^\tau \tilde{R}(\bar{\tau}) \sqrt{\tau - \bar{\tau}} \mathcal{H}\left(\frac{\xi}{\sqrt{\tau - \bar{\tau}}}\right) \mathrm{d}\bar{\tau}. \tag{28}$$

The dimensionless curvature is obtained by differentiation of (28),

$$\partial_\xi^2 \eta(\xi, \tau) = \frac{1}{2\sqrt{2\pi}} \int_0^\tau \frac{\tilde{R}(\bar{\tau})}{\sqrt{\tau - \bar{\tau}}} \left[\sin\left(\frac{\xi^2}{4(\tau - \bar{\tau})}\right) - \cos\left(\frac{\xi^2}{4(\tau - \bar{\tau})}\right)\right] \mathrm{d}\bar{\tau}. \tag{29}$$

In particular, the dimensionless curvature at the contact point is given by

$$\partial_\xi^2 \eta\left(0,\tau\right) = \frac{-1}{2\sqrt{2\pi}} \int_0^\tau \frac{\tilde{R}\left(\bar{\tau}\right)}{\sqrt{\tau-\bar{\tau}}} \mathrm{d}\bar{\tau}. \tag{30}$$

4.3 Pattern 2: Double contact

In another contact pattern, the contact between the beam and the wall consists in two symmetric concentrated forces, located at $\xi = \pm\lambda_c\left(\tau\right)$ and moving away from each other, see Fig. 2. In this case, the reaction is written as a sum of two Dirac functions and the governing equation reads

$$\partial_\tau^2 \eta + \partial_\xi^4 \eta = \frac{1}{2}\tilde{R}\left(\tau\right)\delta\left(\xi - \lambda_c\left(\tau\right)\right) + \frac{1}{2}\tilde{R}\left(\tau\right)\delta\left(\xi + \lambda_c\left(\tau\right)\right) \tag{31}$$

with $\tilde{R}(\tau)$ the total reaction on the wall. In this case, the response reads

$$\eta\left(\xi,\tau\right) = \frac{1}{2}\int_0^\tau \tilde{R}\left(\bar{\tau}\right)\left[\mathcal{K}\left(\xi - \lambda_c\left(\bar{\tau}\right),\tau-\bar{\tau}\right) + \mathcal{K}\left(\xi + \lambda_c\left(\bar{\tau}\right),\tau-\bar{\tau}\right)\right]\mathrm{d}\bar{\tau}. \tag{32}$$

The dimensionless curvature of the beam is obtained after two differentiations with respect to ξ. In particular, for $\xi = 0$,

$$\partial_\xi^2 \eta\left(0,\tau\right) = \frac{1}{\sqrt{2\pi}}\int_0^\tau \frac{\tilde{R}\left(\bar{\tau}\right)}{\sqrt{\tau-\bar{\tau}}}\mathcal{H}''\left(\frac{\lambda_c\left(\bar{\tau}\right)}{\sqrt{\tau-\bar{\tau}}}\right)\mathrm{d}\bar{\tau}. \tag{33}$$

5 Perturbation analysis solution

5.1 General equations

The problem at hand is governed by the linear partial differential equation (9), supplemented with the complementarity condition (18). Perturbation approaches are not well documented for linear complementarity problems. However, as seen next, it seems that standard methods in perturbation methods could provide an interesting approach to the solution of this class of problems. Considering the usual ansatz

$$\eta = \eta_0 + \varepsilon\eta_1 + \varepsilon^2\eta_2^2 + \ldots, \tag{34}$$

substituting this ansatz into the governing equation and balancing the similar powers of ε yields

$$\mathrm{ord}(\varepsilon^0): \quad \partial_\tau^2\eta_0 + \partial_\xi^4\eta_0 = \tilde{r}_0 \tag{35}$$

$$\mathrm{ord}(\varepsilon^1): \quad \partial_\tau^2\eta_1 + \partial_\xi^4\eta_1 = \tilde{r}_1 \tag{36}$$

$$\vdots$$

where the expansion

$$\tilde{r} = \tilde{r}_0 + \varepsilon\tilde{r}_1 + \varepsilon^2\tilde{r}_2^2 + \ldots \tag{37}$$

is naturally considered for the unknown reaction on the wall. This a priori unknown reaction satisfies the complementarity condition (18) which is also considered at the different orders:

$$\mathrm{ord}(\varepsilon^0): \quad \eta_0(\xi,\tau) = \nu\tau - \kappa\frac{\xi^2}{2} \tag{38}$$

$$\mathrm{ord}(\varepsilon^1): \quad \eta_1(\xi,\tau) = \psi\frac{\xi^4}{24} + \chi\frac{\xi^2\tau}{2} + \alpha\frac{\tau^2}{2} \tag{39}$$

$$\vdots$$

At leading order, the governing equation (35) needs to be solved together with the complementarity equation (38) which should be satisfied for $\xi \in \mathcal{D}(\tau)$. Two different scenarii are possible: the impact results either in a discrete contact $\mathcal{D} = \{0\}$, either a double contact at the edges of domain $\mathcal{D} = [-\lambda_c(\tau), \lambda_c(\tau)]$.

5.2 Impact initiated with a discrete contact

Let us first consider the case where a discrete contact is initiated at time $t = 0$. A reaction force $\tilde{R}_0(\tau)$ develops and the fast dynamics solution is given by (28). In particular, at the contact point ($\xi = 0$),

$$\eta_0(0,\tau) = \int_0^\tau \tilde{R}_0(\bar{\tau})\sqrt{\frac{\tau-\bar{\tau}}{2\pi}}\mathrm{d}\bar{\tau}. \tag{40}$$

Substitution into the complementary condition (38) yields

$$\int_0^\tau \tilde{R}_0(\bar{\tau})\sqrt{\frac{\tau-\bar{\tau}}{2\pi}}\mathrm{d}\bar{\tau} = \nu\tau. \tag{41}$$

This Volterra equation of the first kind for $\tilde{R}_0(\bar{\tau})$ admits a solution in the form

$$\tilde{R}_0(\tau) = 2\sqrt{\frac{2}{\pi}}\frac{r_0}{\sqrt{\tau}}. \tag{42}$$

Indeed, by substituting this ansatz into the equation above, the integral is evaluated to $r_0\tau$, which shows that the complementarity condition is trivially satisfied by choosing

$$r_0 = \nu. \tag{43}$$

Because $\nu > 0$, the wall reaction is indeed positive at leading order. It decreases as $r_0\tau^{-1/2}$. Putting all arguments together, the fast dynamics solution (28) is finally given by

$$\eta(\xi,\tau) = \frac{2\nu}{\pi}\int_0^\tau \sqrt{\frac{\tau-\bar{\tau}}{\bar{\tau}}}\mathcal{H}\left(\frac{\xi}{\sqrt{\tau-\bar{\tau}}}\right)\mathrm{d}\bar{\tau}. \tag{44}$$

This discrete contact solution ceases to be valid as soon as the total curvature of the beam at the contact point vanishes, after which the beam unfolding is completed and a continuous contact pattern takes place. The total curvature of the beam, $\kappa + \partial_\xi^2\eta(0,\tau)$, is obtained by adding the initial (slow timescale) curvature

and the curvature associated with the response under the reaction force. The later is expressed by (30) with the reaction force given by (42),

$$\kappa - \frac{1}{2\sqrt{2\pi}} \int_0^\tau \frac{\tilde{R}\left(\bar{\tau}\right) d\bar{\tau}}{\sqrt{\tau - \bar{\tau}}} = \kappa - \frac{r_0}{\pi} \int_0^\tau \frac{d\bar{\tau}}{\sqrt{\bar{\tau}}\sqrt{\tau - \bar{\tau}}} = \kappa - \frac{\nu}{\pi} \int_0^1 \frac{d\gamma}{\sqrt{\gamma}\sqrt{1-\gamma}} = \kappa - \nu. \tag{45}$$

Interestingly, the total curvature remains constant, at leading order, in the post-impact phase with a single discrete contact. Consequently, whether the contact pattern is a discrete or a continuous (double force) pattern, only depends on $\kappa - \nu$, and does not change, at leading order, during the post-impact phase. For small impact velocity, $0 < \nu \leq \kappa$, a single contact develops. For large impact velocity, $\kappa < \nu$, a double contact pattern develops. This solution is studied in the following Section.

5.3 Impact initiated with a double contact

When $\kappa < \nu$, the impact velocity is so high that the beam instantaneously unfolds. A continuous contact between the beam and the wall develops, over a finite distance $\xi \in [-\lambda_c(\tau)\,;\lambda_c(\tau)]$. In the most general case, the reaction $r(\xi)$ is composed of two discrete forces at the extremities and a distributed pressure in-between. We show that this distributed pressure is equal to zero for constant velocity impact, at leading. Indeed, along the contact domain $\mathcal{D}(\tau) = [-\lambda_c(\tau)\,;\lambda_c(\tau)]$, the deformed configuration of the beam complies with the geometry of the wall so that (38) holds over the finite domain $\mathcal{D}$, i.e. $\eta_0(\xi,\tau) = \nu\tau - \kappa\xi^2/2$. Substituting this expression for $\eta_0(\xi,\tau)$ in the governing equation (35) yields $\tilde{r}_0 = 0$, which indicates that there is no distributed reaction on the wall.

The reaction pattern therefore simply consists in two traveling forces which are symmetrically *ejected* from abscissa $\xi = 0$ at time $\tau = 0$, and are located at the ends of the growing contact region. The portion of beam left in-between is instantaneously at rest as it reaches the wall, as a consequence of the traveling forces. The magnitude $\tilde{R}_0(\tau)$ and the locations $\pm\lambda_c(\tau)$ of these contact forces are determined next.

The deformed configuration is given by equation (32), and in particular, for $\xi = 0$,

$$\eta_0(0,\tau) = \int_0^\tau \tilde{R}_0\left(\bar{\tau}\right) \mathcal{K}\left(\lambda_c\left(\bar{\tau}\right), \tau - \bar{\tau}\right) \mathrm{d}\bar{\tau} \tag{46}$$

which should be equal to $\nu\tau$ to meet the complementarity equation. This is another integral equation in the two unknowns $\tilde{R}_0(\tau)$ and $\lambda_c(\tau)$. Seeking again a solution in the form (42), this yields

$$\frac{2r_0}{\pi} \int_0^\tau \sqrt{\frac{\tau - \bar{\tau}}{\bar{\tau}}} \mathcal{H}\left(\frac{\lambda_c\left(\bar{\tau}\right)}{\sqrt{\tau - \bar{\tau}}}\right) \mathrm{d}\bar{\tau} = \nu\tau. \tag{47}$$

The integral on the left can be rewritten with the scaled time $\gamma = \bar{\tau}/\tau$,

$$\frac{2}{\pi} r_0 \tau \int_0^1 \sqrt{\frac{1-\gamma}{\gamma}} \mathcal{H}\left(\frac{\sqrt{\gamma}}{\sqrt{1-\gamma}} \frac{\lambda_c(\gamma\tau)}{\sqrt{\gamma\tau}}\right) \mathrm{d}\gamma = \nu\tau. \tag{48}$$

This expression shows that the result of the integral should be trivially independent of τ. This is only possible if the argument of $\mathcal{H}[\cdot]$ is independent of τ, which yields the functional form

$$\lambda_c(\tau) = \lambda_0\sqrt{\tau}. \tag{49}$$

This indicates that the contact length grows like $\sqrt{\tau}$ at leading order. The velocity at which the contact length increases is therefore infinite when contact occurs, hence the use of wording 'ejection'. Substituting this form for $\lambda_c(\tau)$ into (47), and considering the change of variable

$$\beta = \sqrt{\frac{\bar{\tau}}{\tau - \bar{\tau}}}, \tag{50}$$

the complementarity condition at $\xi = 0$ becomes

$$\frac{2r_0}{\pi} \int_0^{+\infty} \frac{2\tau \mathcal{H}(\lambda_0 \beta)}{(1+\beta^2)^2} \mathrm{d}\beta = \nu\tau. \tag{51}$$

Simplification by τ yields

$$r_0 \, \varphi_\nu(\lambda_0) = \nu, \tag{52}$$

where $\varphi_\nu(\lambda)$ is defined as

$$\varphi_\nu(\lambda) := \frac{4}{\pi} \int_0^{+\infty} \frac{\mathcal{H}(\lambda\beta)}{(1+\beta^2)^2} \mathrm{d}\beta \tag{53}$$

This function is explicitly given in Appendix A and represented in Figure 4-a.

A second equation to determine r_0 and λ_0 is obtained by enforcing that the two traveling forces are such that the curvature of the beam is equal to the (zero) curvature of the wall along the contact. This is expressed by substituting (42) into (33). In particular, this curvature compliance should be valid for $\xi = 0$. Specifying (20) for $\xi = 0$ and using (46) for η_0 yields

$$\partial_\xi^2 \eta_0(0,\tau) = \frac{2}{\pi} \int_0^{\tau} \frac{r_0}{\sqrt{\bar{\tau}(\tau - \bar{\tau})}} \mathcal{H}'' \left(\lambda_0 \sqrt{\frac{\bar{\tau}}{\tau - \bar{\tau}}} \right) \mathrm{d}\bar{\tau} = -\kappa. \tag{54}$$

Introducing the same change of variable $\beta = \sqrt{\bar{\tau}/(\tau - \bar{\tau})}$ as before, this condition becomes

$$r_0 \, \varphi_\kappa(\lambda_0) = \kappa \tag{55}$$

where $\varphi_\kappa(\lambda)$ is defined as

$$\varphi_\kappa(\lambda) := -\frac{4}{\pi} \int_0^{+\infty} \frac{\mathcal{H}''(\lambda\beta)}{1+\beta^2} \mathrm{d}\beta = \frac{8}{\pi\lambda^2} \int_0^{+\infty} \frac{\left(1 - 3\beta^2\right) \mathcal{H}(\lambda\beta)}{(1+\beta^2)^3} \mathrm{d}\beta, \tag{56}$$

and where the second equality is obtained after two integrations by parts. This function is explicitly given in Appendix A and represented in Figure 4-a.

Equations (52) and (55) form a set of two algebraic transcendental equations in the unknowns r_0 and λ_0 which govern the magnitude and position of the two reactions on the wall, at leading order. Eliminating r_0 readily provides a single equation in λ_0,

$$\frac{\varphi_\kappa(\lambda_0)}{\varphi_\nu(\lambda_0)} = \frac{\kappa}{\nu}. \tag{57}$$

Evaluation of r_0 then follows by back-substitution in either (52) or (55). By noticing that $\varphi_\kappa(\lambda_0)/\varphi_\nu(\lambda_0)$ is monotonically decreasing from 1 (for $\lambda_0 = 0$) to 0 as $\lambda_0 \to +\infty$, see Figure 4-a, and recalling that

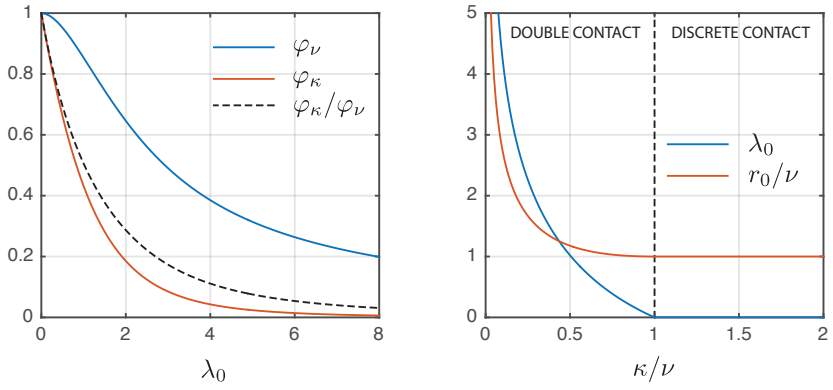

Fig. 4: (a) Functions φ_ν and φ_κ which are used to solve the problem at leading order; (b) Solutions λ_0 and r_0/ν. of the double contact problem.

κ/ν	0	0.02	0.04	0.06	0.08	0.1	0.2	0.3	0.4	0.5	0.6	0.7	0.8	0.9	1
λ_0	∞	9.976	7.007	5.661	4.837	4.258	2.704	1.916	1.398	1.019	0.725	0.490	0.297	0.136	0
r_0/ν	∞	6.259	4.412	3.585	3.088	2.745	1.885	1.511	1.304	1.177	1.098	1.048	1.019	1.004	1

Tab. 1: Some numerical values for λ_0 and r_0/ν, given as a function of κ/ν.

the double contact solution only occurs for $\nu > \kappa$, we see that the problem possesses a unique solution. Furthermore, for $\kappa/\nu = 1$, the solution is $\lambda_0 = 0$ and $r_0 = \nu(= \kappa)$, which is consistent with the discrete contact solution developed previously. For other values of κ/ν, Figure 4-b shows the solutions λ_0 and r_0/ν. Table 1 summarizes some numerical values.

The values of the two unknowns r_0 and λ_0 have been obtained by expressing the complementarity condition at $\xi = 0$, in both the strict and weak senses. Since the derivation was obtained for an assumed functional form for $R_0(\tau)$, it is necessary to show that the complementarity condition is satisfied everywhere along the contact domain $\mathcal{D}(\tau)$, not only for $\xi = 0$. This proof involves heavier mathematical derivations, given in Appendix B. This being proved, the contact problem initiated with a double contact force pattern admits therefore the unique solution

$$\eta(\xi,\tau) = \frac{r_0}{\pi}\int_0^\tau \sqrt{\frac{\tau-\bar\tau}{\bar\tau}}\left[\mathcal{H}\left(\frac{\xi-\lambda_0\sqrt{\bar\tau}}{\sqrt{\tau-\bar\tau}}\right)+\mathcal{H}\left(\frac{\xi+\lambda_0\sqrt{\bar\tau}}{\sqrt{\tau-\bar\tau}}\right)\right]\mathrm{d}\bar\tau, \tag{58}$$

valid , $\forall\xi\in\mathbb{R}$, $\tau>0$. When $\lambda_0 = 0$ and $r_0 = \nu$, this expression degenerates into (44).

6 Discussion

6.1 Illustration

Figure 5 illustrates the different types of solutions observed in the beam-wall interaction problem. The left panels depict an impact initiated with a discrete contact ($\nu < \kappa$), while the right panels show an impact characterized by a double contact ($\nu > \kappa$). In all cases, the macroscopic solution, $\nu\tau - \frac{\kappa\xi^2}{2}$, is represented by blue dashed lines. This macroscopic solution corresponds to the configuration of the beam that would continue to move as a rigid body if the wall were absent. Snapshots are provided for $\tau \in \{0.1, 0.25, 0.5\}$.

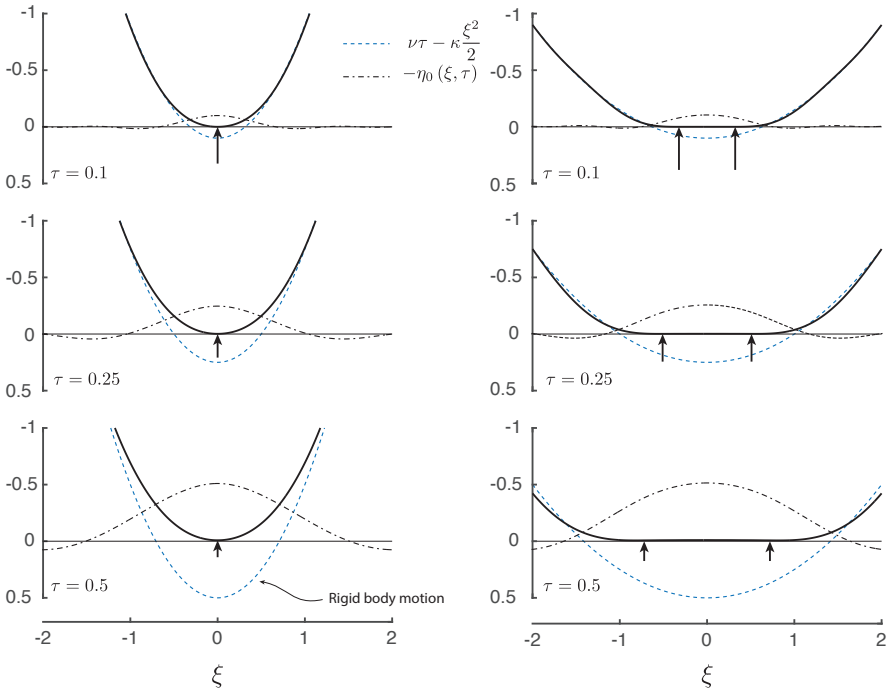

Fig. 5: Leading order solution of the beam impacting a rigid wall. Snapshots of the solution at time $\tau = 0.1,\ 0.25,\ 0.5$ for an impact velocity $\nu = 1$ (a) Discrete contact, $\kappa = 2(\geq \nu)$; (b) Double contact, $\kappa = 0.5(\leq \nu)$

The negative of the fast dynamics response, $-\eta_0(\xi,\tau)$, is represented by dash-dot lines. The expressions for η_0 are provided in Eqs. (44) and (58) for the cases of discrete and double contact, respectively.

The actual deformation of the beam is the sum of the macroscopic rigid body motion and the fast dynamics response. For discrete contact, the evolution of the reaction force, which is proportional to $1/\sqrt{\tau}$, ensures that the contact point remains fixed after the initial contact. The magnitude of the force is indicated by the size of the arrows in the figure. For the double contact case, the decrease in the contact reaction force, combined with the splitting of the two contact forces that localize at a growing distance $\lambda_c \sim \sqrt{\tau}$, ensures that the segment of the beam between the two contact forces remains stationary and maintains perfect contact with the rigid wall following the impact.

6.2 Beyond the leading order solution

The solution presented earlier corresponds to the leading-order approximation, which simplifies the problem by considering an infinite beam with constant curvature and velocity. Extending this analysis to higher-order corrections introduces additional terms involving higher-order time and space derivatives. Specifically, these include the acceleration (α), the fourth-degree spatial derivative (ψ), and the rate of change of curvature (χ). These dimensionless quantities, defined in Equation (18), enable matching between the fast and slow dynamics, thus providing a more comprehensive description of the system's behavior. While a formal proof lies beyond the scope of this study, it is reasonable to hypothesize that the corrections are described with a Frobenius series expansion. For example, in the case of discrete contact, the reaction force could be expanded as $R_0 \sim \frac{1}{\sqrt{\tau}}(\nu + \varepsilon\alpha\tau + \cdots)$.

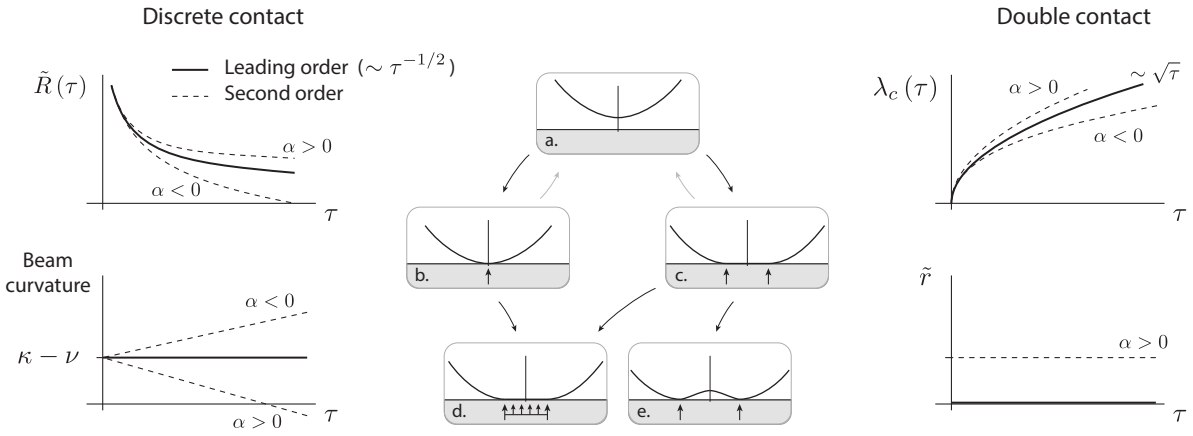

Fig. 6: Overview of contact patterns and possible transitions. a. no contact, b. discrete contact, c. double contact without wall pressure, d. double contact with pressure on wall, e. double contact with detached contact in-between.

At leading order, the reaction force decreases proportionally to $\nu\tau^{-1/2}$. However, as τ approaches $1/\varepsilon$, the first correction becomes significant. When the acceleration parameter α is positive, the reaction force initially increases, and the curvature at the contact point decreases. This behavior can potentially cause a transition from a discrete to a distributed contact pattern, a transition that is not captured by the leading-order solution for which the total beam curvature is an invariant. Conversely, for negative acceleration toward the wall ($\alpha < 0$), the reaction force decays more rapidly, eventually becoming negative and leading to detachment of the beam from the support, returning to a contact-free configuration as illustrated in Figure 6. This latter phenomenon, however, is practically less relevant, as the time required for detachment ($-\nu/(\varepsilon\alpha)$) is comparable to the macroscopic timescale, invalidating the timescale separation assumption. In very specific scenarios where $|\alpha| \gg \nu$, corresponding to grazing impacts with small finite momentum transfer, the duration of the contact is short enough so that the multiple timescale analysis remains valid. In all other cases, the model remains limited in its ability to fully describe scenarios involving beam rebound or long-duration interactions.

A notable feature of the higher-order correction arises in the context of continuous contact. While the leading-order reaction pattern consists solely of two concentrated forces at the contact points (pattern c. in Figure 6), higher-order corrections introduce a distributed pressure between these points. This distributed pressure stems from the compatibility condition along the finite contact length. Substituting the higher-order expression for the deformation (18) into the governing equation (9) reveals that the distributed reaction force is given by $\tilde{r} = \varepsilon(\psi + \alpha)$. The behavior of the beam between the two concentrated forces is thus determined by the sign of $\psi + \alpha$. A positive value indicates a pressing distributed contact on the wall (pattern d. in Figure 6) while a negative value is not physically acceptable and actually results in a detached zone between the two contact points (pattern e. in Figure 6).

Overall, the higher-order analysis can result in additional contact patterns that are inaccessible in the leading-order solution, as illustrated in Figure 6.

6.3 Utility of the current solution in numerical methods

The results presented in this study offer significant potential utility for applied mathematicians developing numerical techniques, particularly in two specific contexts.

The first application involves using the analytical solutions developed herein to validate numerical codes. A particularly challenging scenario for numerical methods is the case of constant velocity impact. Theoretically, this scenario results in a portion of the beam remaining in continuous contact with the rigid wall but without any reaction force over a finite length. Capturing this behavior accurately is inherently difficult for numerical methods. Numerically, the absence of a reaction force may be misrepresented as either a small penetration of the wall, resulting in an artificial non-zero reaction force, or as a detached configuration, creating a slight gap between the beam and the wall. Both artifacts could potentially be controlled by refining the numerical discretization, but they remain indicative of the difficulty in resolving this behavior. Additionally, the presence of local penetration or detachment, arising from numerical artifacts, is unlikely to be uniformly distributed along the contact length. This could lead to high-frequency, short-wavelength perturbations superimposed on the expected theoretical solution, further complicating the numerical representation of the problem.

Along the same line, the current solutions highlight two clearly different contact patterns, discrete vs. continuous contact, and capturing appropriately the transition from one pattern to the other is something that could be used for benchmarking numerical codes.

The solutions derived in this paper could also potentially improve existing numerical methods by incorporating insights from the analytical solutions. A critical challenge in numerical simulations of beam impact is accurately capturing the rapid transfer of momentum as contact occurs. Theoretically, the reaction force is both initially infinite and rapidly decreasing, necessitating extremely small time steps in numerical simulations to resolve this behavior accurately. The analytical solutions derived in this study offer an opportunity to relax this constraint, especially by providing asymptotic solutions as a function of known macroscopic quantities such as the impact velocity and the beam curvature at impact. By embedding these solutions into numerical models, it may be possible to bypass the need for excessively small time steps and instead employ more macroscopic timesteps. For instance, an analytical sub-model could describe the reaction force and momentum transfer over the initial phases of contact, allowing the numerical simulation to focus on the subsequent dynamics at a coarser temporal resolution. While this paper does not aim to develop a novel numerical methodology, these perspectives highlight the potential for advancing numerical simulations in impact mechanics.

7 Conclusions

The impact of a compliant structure against a rigid obstacle is characterized by multiple time and spatial scales, from rapid local deformations and stress wave propagation to slower global motions. These scales pose significant challenges for numerical methods in accurately and efficiently capturing the short-time response near the point of contact. In this paper, we addressed this problem using a beam impacting a rigid obstacle as a minimal yet illustrative example of such multi-scale phenomena.

We derived a local asymptotic solution for the short-time response, leveraging the separation of time and spatial scales. At leading order, this analysis reveals two distinct contact patterns, determined by the ratio of the impact velocity to the curvature of the beam at the point of impact. For low impact velocity or high curvature, a single concentrated contact force develops and decreases with the inverse square root of time. For higher velocities or lower curvature, the contact splits into two traveling forces that move apart at a rate inversely proportional to the square root of time. Notably, in the latter case, the beam segment between the two forces remains at rest, presenting unique challenges for numerical methods, particularly those relying on penetration conditions to enforce contact.

This work highlights the existence of bifurcation in contact patterns based on simple parameters, offering new insights into the dynamic response of compliant structures during impact. The solution

presented in this study can serve as a valuable benchmark for evaluating and improving numerical methods, particularly in scenarios where capturing singular responses and multi-scale phenomena is critical. Future work could explore how these findings might be integrated into computational frameworks to enhance their accuracy and efficiency in handling such complex dynamics.

Acknowledgements

This work was partly carried out while the first author was an MTS Visiting Professor at the University of Minnesota, and during a UPS Visiting Professor appointment at Stanford University.

References

[1] William James Stronge. *Impact Mechanics*. Cambridge University Press, Cambridge, online-ausg edition, 2000.

[2] C.C. Fu. Closed-form solutions of an infinite beam under impact loading. *International Journal of Solids and Structures*, 3(4):607–615, July 1967.

[3] S. Ranganath. Normal Impact of an Infinite Elastic Beam by a Semi-Infinite Elastic Rod. *Journal of Applied Mechanics*, 38(2):455–460, June 1971.

[4] Karl F. Graff. *Wave motion in elastic solids*. Ohio State Univ. Press, Columbus, 1975.

[5] Minggang Zhou and William P. Schonberg. Comment on global/local method for low-velocity impact problems. *Journal of Engineering Mechanics*, 120(5):1042–1056, May 1994.

[6] Olivier A. Bauchau. Analysis of Flexible Multibody Systems with Intermittent Contacts. *Multibody System Dynamics*, 4(1):23–54, February 2000.

[7] Qiong-Zhong Chen, Vincent Acary, Geoffrey Virlez, and Olivier Brüls. A nonsmooth generalized α scheme for flexible multibody systems with unilateral constraints. *International Journal for Numerical Methods in Engineering*, 96(8):487–511, November 2013.

[8] Damien Durville. Contact-friction modeling within elastic beam assemblies: an application to knot tightening. *Computational Mechanics*, 49(6):687–707, June 2012.

[9] Florence Bertails-Descoubes, Florent Cadoux, Gilles Daviet, and Vincent Acary. A nonsmooth Newton solver for capturing exact Coulomb friction in fiber assemblies. *ACM Transactions on Graphics*, 30(1):1–14, January 2011.

[10] Jeongho Ahn and David E. Stewart. An Euler–Bernoulli Beam with Dynamic Contact: Discretization, Convergence, and Numerical Results. *SIAM Journal on Numerical Analysis*, 43(4):1455–1480, January 2005.

[11] Elisabet V. Lens and Alberto Cardona. A nonlinear beam element formulation in the framework of an energy preserving time integration scheme for constrained multibody systems dynamics. *Computers & Structures*, 86(1-2):47–63, January 2008.

[12] T.C. Soong and Injae Choi. An elastica that involves continuous and multiple discrete contacts with a boundary. *International Journal of Mechanical Sciences*, 28(1):1–10, January 1986.

[13] V. Denoël. Advantages of a semi-analytical approach for the analysis of an evolving structure with contacts. *Communications in Numerical Methods in Engineering*, 24(12):1667–1683, December 2008.

[14] Vincent Denoël and Emmanuel Detournay. Eulerian formulation of constrained elastica. *International Journal of Solids and Structures*, 48(3-4):625–636, February 2011.

[15] Jen-San Chen. On the contact behavior of a buckled Timoshenko beam constrained laterally by a plane wall. *Acta Mechanica*, 222(3-4):225–232, December 2011.

[16] Anna Liakou and Emmanuel Detournay. Constrained buckling of variable length elastica: Solution by geometrical segmentation. *International Journal of Non-Linear Mechanics*, 99:204–217, 2018.

[17] Alexandre Depouhon, Emmanuel Detournay, and Vincent Denoël. Accuracy of one-step integration schemes for damped/forced linear structural dynamics. *International Journal for Numerical Methods in Engineering*, 99(5):333–353, August 2014.

[18] Jae Hyung Kim, Young Ju Ahn, Yong Hoon Jang, and J.R. Barber. Contact problems involving beams. *International Journal of Solids and Structures*, 51(25-26):4435–4439, December 2014.

[19] NIST Digital Library of Mathematical Functions. *NIST Digital Library of Mathematical Functions*. National Institute of Standards and Technology, 2023. Release 1.1.9 of 2023-06-15.

Appendix A

Functions $\varphi_\nu(\lambda)$ and $\varphi_\kappa(\lambda)$ that have been introduced in (53) and (56) admit the following expressions as a function of the Fresnel integrals of the first kind $\mathcal{S}(\cdot)$ and $\mathcal{C}(\cdot)$:

$$\varphi_\nu(\lambda) = \frac{4}{\pi}\int_0^{+\infty} \frac{\mathcal{H}(\lambda\beta)}{(1+\beta^2)^2}\mathrm{d}\beta = \cos\left(\frac{\lambda^2}{4}\right)\left[1-2\mathcal{S}\left(\frac{\lambda}{\sqrt{2\pi}}\right)\right] - \sin\left(\frac{\lambda^2}{4}\right)\left[1-2\mathcal{C}\left(\frac{\lambda}{\sqrt{2\pi}}\right)\right] \tag{59}$$

$$\varphi_\kappa(\lambda) = -\frac{4}{\pi}\int_0^{+\infty} \frac{\mathcal{H}''(\lambda\beta)}{1+\beta^2}\mathrm{d}\beta = \cos\left(\frac{\lambda^2}{4}\right)\left[1-2\mathcal{C}\left(\frac{\lambda}{\sqrt{2\pi}}\right)\right] + \sin\left(\frac{\lambda^2}{4}\right)\left[1-2\mathcal{S}\left(\frac{\lambda}{\sqrt{2\pi}}\right)\right] \tag{60}$$

Appendix B

In the configuration with two contact forces, the values of r_0 and λ_0 have been determined by enforcing the complementarity conditions at $\xi = 0$, both for η_0 and $\partial_\xi^2\eta_0$. It is necessary to verify that the ansatz (42) used for the reaction and these values of r_0 and λ_0 provide a solution that satisfies the complementarity condition all along the contact, i.e. $\forall\xi \in [-\lambda_c(\tau), \lambda_c(\tau)]$. In a first step, we verify that the solution is indeed valid for $\xi = \lambda_c(\tau) = \lambda_0\sqrt{\tau}$ where the fast dynamics displacement reads

$$\eta_0\left(\lambda_0\sqrt{\tau},\tau\right) = \frac{r_0}{\pi}\int_0^{\tau}\sqrt{\frac{\tau-\bar\tau}{\bar\tau}}\left[\mathcal{H}\left(\lambda_0\frac{\sqrt{\tau}-\sqrt{\bar\tau}}{\sqrt{\tau-\bar\tau}}\right)+\mathcal{H}\left(\lambda_0\frac{\sqrt{\tau}+\sqrt{\bar\tau}}{\sqrt{\tau-\bar\tau}}\right)\right]d\bar\tau. \tag{61}$$

Considering the changes of variable $\beta_\pm = \frac{\sqrt{\tau}\pm\sqrt{\bar{\tau}}}{\sqrt{\tau-\bar{\tau}}}$ for the two terms in the brackets above, respectively, a similar integrand is obtained,

$$\int_0^\tau \sqrt{\frac{\tau-\bar{\tau}}{\bar{\tau}}}\mathcal{H}\left(\lambda_0\frac{\sqrt{\tau}+\sqrt{\bar{\tau}}}{\sqrt{\tau-\bar{\tau}}}\right)d\bar{\tau} = 16\tau\int_1^\infty \frac{\beta_+^2\mathcal{H}\left(\lambda_0\beta_+\right)}{\left(1+\beta_+^2\right)^3}d\beta_+ \tag{62}$$

$$\int_0^\tau \sqrt{\frac{\tau-\bar{\tau}}{\bar{\tau}}}\mathcal{H}\left(\lambda_0\frac{\sqrt{\tau}-\sqrt{\bar{\tau}}}{\sqrt{\tau-\bar{\tau}}}\right)d\bar{\tau} = 16\tau\int_0^1 \frac{\beta_-^2\mathcal{H}\left(\lambda_0\beta_-\right)}{\left(1+\beta_-^2\right)^3}d\beta_- \tag{63}$$

while one change of variables maps the interval $[0;\tau]$ onto $[0;1]$ and the other onto $[1;+\infty]$, so that merging them yields

$$\eta_0\left(\lambda_0\sqrt{\tau},\tau\right) = \frac{16}{\pi}r_0\tau\int_0^\infty \frac{\beta^2\mathcal{H}\left(\lambda_0\beta\right)}{\left(1+\beta^2\right)^3}\mathrm{d}\beta. \tag{64}$$

It is now required to check whether this compensates the slow dynamics solution, expressed with the fast coordinates, i.e.

$$\nu\tau - \kappa\frac{\xi^2}{2} = \nu\tau - \kappa\frac{\lambda_0^2\tau}{2} = r_0\tau\left(\varphi_\nu\left(\lambda_0\right) - \varphi_\kappa\left(\lambda_0\right)\frac{\lambda_0^2}{2}\right). \tag{65}$$

Introducing the definitions (53) and (56) for φ_ν and φ_κ, we obtain

$$r_0\tau\left(\varphi_\nu\left(\lambda_0\right) - \varphi_\kappa\left(\lambda_0\right)\frac{\lambda_0^2}{2}\right) = \frac{4}{\pi}r_0\tau\int_0^{+\infty}\frac{\mathcal{H}\left(\lambda_0\beta\right)}{\left(1+\beta^2\right)^2} - \frac{\left(1-3\beta^2\right)\mathcal{H}\left(\lambda_0\beta\right)}{\left(1+\beta^2\right)^3}\mathrm{d}\beta = \frac{16}{\pi}r_0\tau\int_0^{+\infty}\frac{\beta^2\mathcal{H}\left(\lambda_0\beta\right)}{\left(1+\beta^2\right)^3}\mathrm{d}\beta. \tag{66}$$

Comparison with (64) confirms that the complementarity condition is also satisfied at the ends of the contact.

In a second stage, we prove that the complementarity condition is also satisfied all along the contact, by considering a generic expression $\xi = \lambda_0\zeta\sqrt{\tau}$, with $\zeta \in [-1;1]$. For symmetry reason, only positive values of ζ will be considered. Using the change of variable $\bar{\tau} = \gamma\,\tau$, the fast dynamics displacement reads

$$\eta_0\left(\zeta,\tau\right) = \frac{r_0\tau}{\pi}\int_0^1\sqrt{\frac{1-\gamma}{\gamma}}\left[\mathcal{H}\left(\lambda_0\frac{\zeta+\sqrt{\gamma}}{\sqrt{1-\gamma}}\right) + \mathcal{H}\left(\lambda_0\frac{\zeta-\sqrt{\gamma}}{\sqrt{1-\gamma}}\right)\right]\mathrm{d}\gamma \tag{67}$$

This integral is composed of two terms. The explicit computation of each term is likely not tractable. Nevertheless conveniently splitting this integral into three parts

$$\eta_0\left(\zeta,\tau\right) = I_1\left(\zeta,\tau\right) + I_2\left(\zeta,\tau\right) + I_3\left(\zeta,\tau\right) \tag{68}$$

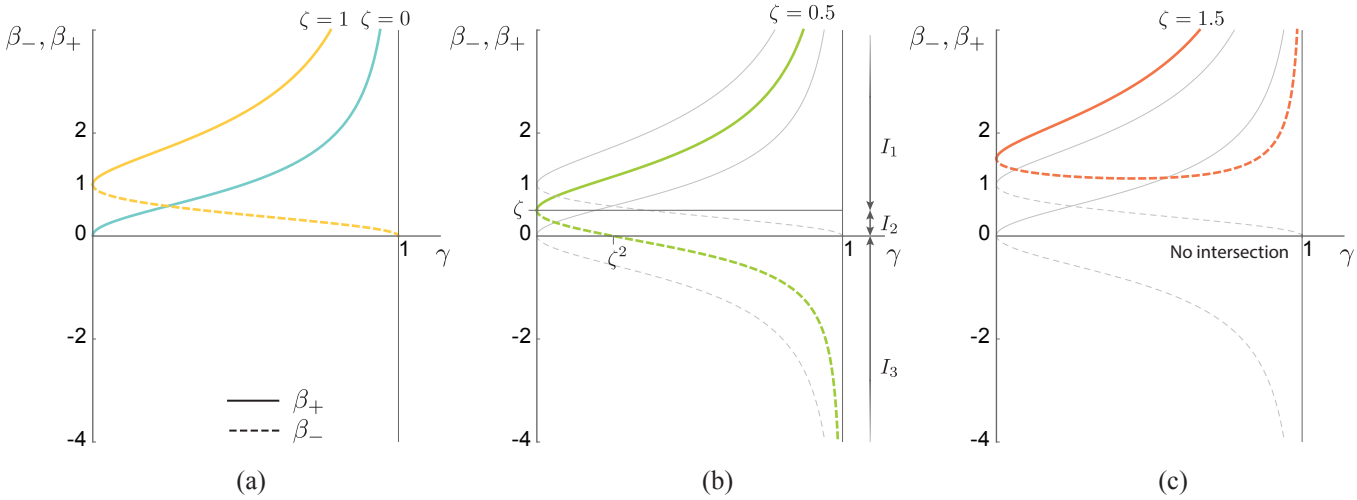

Fig. 7: Illustration of the changes of variable $\beta_-(\gamma)$ and $\beta_+(\gamma)$ used to demonstrate that the complementarity condition holds all along the domain $\mathcal{D}(\tau)$.

where

$$I_1 = \frac{r_0\tau}{\pi}\int_0^1 \sqrt{\frac{1-\gamma}{\gamma}}\mathcal{H}\left(\lambda_0\frac{\zeta+\sqrt{\gamma}}{\sqrt{1-\gamma}}\right)\mathrm{d}\gamma,$$
$$I_2 = \frac{r_0\tau}{\pi}\int_0^{\zeta^2} \sqrt{\frac{1-\gamma}{\gamma}}\mathcal{H}\left(\lambda_0\frac{\zeta-\sqrt{\gamma}}{\sqrt{1-\gamma}}\right)\mathrm{d}\gamma,$$
$$I_3 = \frac{r_0\tau}{\pi}\int_{\zeta^2}^1 \sqrt{\frac{1-\gamma}{\gamma}}\mathcal{H}\left(\lambda_0\frac{\zeta-\sqrt{\gamma}}{\sqrt{1-\gamma}}\right)\mathrm{d}\gamma, \tag{69}$$

allows for some grouping and simplifications that eventually allow the computation of $\eta_0(\zeta,\tau)$, as shown in the rest of this Appendix.

The split of the domain of integration for the last two terms is motivated by the fact that we want to make use of the changes of variable $\beta_+ = \frac{\zeta+\sqrt{\gamma}}{\sqrt{1-\gamma}}$ and $\beta_- = \frac{\zeta-\sqrt{\gamma}}{\sqrt{1-\gamma}}$ so that the arguments of $\mathcal{H}[\cdot]$ are all the same in each integral. Figure 7 sketches these expressions of β_+ and β_- as a function of γ (in solid and dashed lines for each case). For $\zeta = 0$ ($\xi = 0$), the panel (a) shows that only β_+ matters, see (50). For $\zeta = 1$ ($\xi = \lambda_0\sqrt{\tau}$), the two previously used expressions for β_+ and β_- are shown, (62–63). When γ spans the range $[0,1]$, they respectively go from 0 to 1, and 1 to $+\infty$, as seen earlier. In the more general case shown in panel (b), three cases need to be distinguished. Indeed, it is observed that the first transformation, β_+, maps $\gamma \in [0,1]$ onto $\beta_+ \in [\zeta, +\infty]$ and the second one, β_-, maps $\gamma \in [0,1]$ onto $\beta_- \in [-\infty, \zeta]$. Since $\zeta > 0$, the later interval includes $\beta_- = 0$ where the domain of integration is split in order to explicitly obtain a domain running from 0 to $+\infty$, i.e. $\beta \in [0,\zeta] \cup [\zeta, +\infty]$. The pivotal value $\beta_- = 0$ corresponds to $\gamma = \zeta^2$, which explains to chosen decomposition.

The first integral is analyzed with a change of variable $\sqrt{\gamma} = f_+(\beta)$, such that $\beta = \frac{\zeta+\sqrt{\gamma}}{\sqrt{1-\gamma}}$, i.e. $\frac{\zeta+f_+}{\sqrt{1-f_+^2}} = \beta$. Inverting the mapping in these conditions (with $f_+(\beta)$ required to be positive) yields

$$f_+(\beta) = \frac{-\zeta + \beta\sqrt{\Delta}}{\beta^2 + 1} \tag{70}$$

with $\Delta = 1 - \zeta^2 + \beta^2$. It maps $\gamma \in [0,1]$ onto $\beta \in [\zeta, +\infty]$, as required, with positive Jacobian. It is observed that $f_+(\beta) \geq 0$ when $\zeta \geq 0$ for $\beta \in [\zeta, +\infty]$.

Similarly, integrals I_2 and I_3 are solved with a change of variable $\sqrt{\gamma} = f_-(\beta)$, such that $\beta = \frac{\zeta - \sqrt{\gamma}}{\sqrt{1-\gamma}}$, i.e. $\lambda_0 \frac{\zeta - f_-}{\sqrt{1-f_-^2}} = \beta$. The expression of $f_-(\beta)$ is now different for β positive and negative.

$$f_-(\beta) = \begin{cases} \frac{\zeta + \beta\sqrt{\Delta}}{\beta^2+1} & \text{if } \beta \leq 0 \\ \frac{\zeta - \beta\sqrt{\Delta}}{\beta^2+1} & \text{if } \beta \geq 0 \end{cases} \tag{71}$$

These two transformations respectively map $\gamma \in [0, \zeta^2]$ onto $\beta \in [0, \zeta]$ and $\gamma \in [\zeta^2, 1]$ onto $\beta \in [-\infty, 0]$, both with negative Jacobian. Using notation f momentarily to represent either f_+ or f_-, the Jacobian can be expressed as

$$\frac{\mathrm{d}\gamma}{2\sqrt{\gamma}} = f'(\beta)\,\mathrm{d}\beta. \tag{72}$$

Completion of the change of variable will require expressing $\sqrt{1-\gamma}$ for each integral, which can be expressed as a function of β. For the first integral, it is noticed that $\sqrt{1-\gamma} = (\zeta + f_+)/\beta$, while $\sqrt{1-\gamma} = (\zeta - f_+)/\beta$ for the other two. Therefore, using (70)-(71) yields

$$I_1 = \frac{2r_0\tau}{\pi} \int_{\zeta}^{+\infty} \frac{(\zeta + f_+) f_+'}{\beta} \mathcal{H}(\lambda_0\beta)\,\mathrm{d}\beta = \frac{2r_0\tau}{\pi} \int_{\zeta}^{+\infty} \frac{\left(\beta\zeta + \sqrt{\Delta}\right)\left(2\beta\zeta\sqrt{\Delta} + \left(\beta^2-1\right)\zeta^2 + \beta^2 + 1\right)}{\left(\beta^2+1\right)^3\sqrt{\Delta}} \mathcal{H}(\lambda_0\beta)\,\mathrm{d}\beta \tag{73}$$

$$I_2 = \frac{2r_0\tau}{\pi} \int_{0}^{\zeta} \frac{(\zeta - f_-) f_-'}{\beta} \mathcal{H}(\lambda_0\beta)\,\mathrm{d}\beta = \frac{2r_0\tau}{\pi} \int_{0}^{\zeta} \frac{\left(\beta\zeta + \sqrt{\Delta}\right)\left(2\beta\zeta\sqrt{\Delta} + \left(\beta^2-1\right)\zeta^2 + \beta^2 + 1\right)}{\left(\beta^2+1\right)^3\sqrt{\Delta}} \mathcal{H}(\lambda_0\beta)\,\mathrm{d}\beta \tag{74}$$

$$I_3 = \frac{2r_0\tau}{\pi} \int_{-\infty}^{0} \frac{(\zeta - f_-) f_-'}{\beta} \mathcal{H}(\lambda_0\beta)\,\mathrm{d}\beta = \frac{2r_0\tau}{\pi} \int_{-\infty}^{0} \frac{\left(\beta\zeta - \sqrt{\Delta}\right)\left(2\beta\zeta\sqrt{\Delta} - \left(\beta^2-1\right)\zeta^2 - \beta^2 - 1\right)}{\left(\beta^2+1\right)^3\sqrt{\Delta}} \mathcal{H}(\lambda_0\beta)\,\mathrm{d}\beta \tag{75}$$

Interestingly, the integrands in I_1 and I_2 are now the same. These two integrals combine into a single one, on the domain $[0; +\infty]$. Furthermore, integral I_3 can be evaluated on the positive support using the change of variable $\beta \to -\beta$ and the symmetry property $\mathcal{H}(\lambda_0\beta) = \mathcal{H}(-\lambda_0\beta)$, so that

$$\eta_0(\zeta,\tau) = I_1 + I_2 + I_3 = \frac{4r_0\tau}{\pi} \int_{0}^{+\infty} \frac{\left(3\beta^2-1\right)\zeta^2 + \beta^2 + 1}{\left(\beta^2+1\right)^3} \mathcal{H}(\lambda_0\beta)\,\mathrm{d}\beta \tag{76}$$

after putting together (73)-(75), and some simplifications. After comparison with the definitions of φ_ν and φ_κ, it appears that this latter expression coincides with the macroscopic solution, $\nu\tau - \kappa\frac{\xi^2}{2}$, written with $\xi = \lambda_0\zeta\sqrt{\tau}$, i.e.

$$\nu\tau - \kappa\frac{\left(\lambda_0\zeta\sqrt{\tau}\right)^2}{2} = \left(\nu - \kappa\frac{\lambda_0^2\zeta^2}{2}\right)\tau = r_0\tau\left(\varphi_\nu\left(\lambda_0\right) - \varphi_\kappa\left(\lambda_0\right)\frac{\lambda_0^2\zeta^2}{2}\right). \tag{77}$$

The complementarity condition is therefore satisfied all along the contact domain, for $\zeta \geq 0$. The demonstration for $\zeta \leq 0$ is justified by symmetry or obtained following similar arguments.

Finally, Figure 7-c shows that the decomposition of the integral intro three terms, as considered in this Appendix does not hold as soon as $\zeta > 1$, as β_- then does not cross the $\gamma-$axis any longer. Therefore, the complementary condition is only verified along the contact domain $\mathcal{D}$. Despite the fact that a unique expression $\eta_0\left(\xi,\tau\right)$ is used for the deformed configuration everywhere along the beam, it matches the quadratic formulation along $\mathcal{D}\left(\tau\right)$ only, not elsewhere.